

LINEAR ACCELERATOR DESIGN FOR THE LCLS-II FEL FACILITY

P. Emma, J. Frisch, Z. Huang, A. Marinelli, T. Maxwell, H. Loos, Y. Nosochkov, T. Raubenheimer, J. Welch, L. Wang, M. Woodley, SLAC, Stanford, CA 94309, USA
 A. Saini, N. Solyak, FNAL, Batavia, IL 60510, USA
 J. Qiang, M. Venturini, LBNL, Berkeley, CA 94720, USA

Abstract

The LCLS-II is an FEL facility proposed in response to the July 2013 BESAC advisory committee, which recommended the construction of a new FEL light source with a high-repetition rate and a broad photon energy range from 0.2 keV to at least 5 keV. A new CW 4-GeV electron linac is being designed to meet this need, using a superconducting (SC) L-band (1.3 GHz) linear accelerator capable of operating with a continuous bunch repetition rate up to 1 MHz at ~16 MV/m. This new 700-m linac is to be built at SLAC in the existing tunnel, making use of existing facilities and providing two separate FELs, preserving the operation of the existing FEL, which can be fed from either the existing copper or the new SC linac. We briefly describe the acceleration, bunch compression, beam transport, beam switching, and electron beam diagnostics. The high-power and low-level RF, and cryogenic systems are described elsewhere.

INTRODUCTION

The LCLS-II [1] high-repetition rate FEL project at SLAC aims to construct a new superconducting linac composed of TESLA-like RF cavities in continuous wave (CW) operation, in order to accelerate a 1-MHz electron beam to 4 GeV. This new superconducting linac (SC-linac), driven by a new high-rate injector [2], will replace the existing SLAC copper linac in sectors 1-7 (101.6 m/sector), while the remaining Cu RF structures in sectors 7-10 will be removed and replaced with a simple beam pipe and focusing lattice (the “linac extension”). The existing 2-km PEP-II bypass line (suspended from the tunnel ceiling) will be modified to transport electrons from the linac extension in sector 10 through more than 2.5 km and into either of two undulators in the existing LCLS undulator hall. The layout is shown in Figure 1 with the SC-linac in blue at far left and the SXU and HXU undulators at far right. The “linac extension” and “bypass line” are also shown.

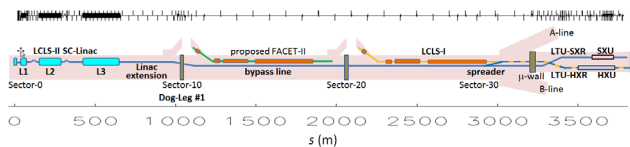


Figure 1: LCLS-II layout in existing SLAC tunnels (3.8 km).

LINAC AND RF LAYOUT

The nominal requirements of this new high-power linac are to accelerate a continuous rate of electron bunches,

with 100 pC per bunch, at a 0.6-MHz repetition rate (or higher with a reduced bunch charge to 10 pC, or lower with 300-pC, maintaining <120 kW in each of two electron dump lines). This new linac makes use of the ‘Tesla-Technology’ accelerating module, with thirty-five 13-m long cryomodules (CM), each including eight 9-cell L-band RF cavities (1.038 m/cavity) cooled to 2.0 K using liquid Helium. In addition, a short 3.9-GHz third-harmonic linac (HL) section is used to linearize the bunch compression process in two short cryomodules, each including eight special 9-cell, 3.9-GHz cavities (0.346 m/cavity) with up to 80 MV of on-crest voltage (decelerating). The linac design includes bunch compressors to nominally produce a 1-kA peak current at 100 pC/bunch without significantly increasing the transverse emittance. Finally, the design must reduce the final correlated energy spread to <0.03% rms and stabilize the beam against the microbunching instability by adding a small intrinsic energy spread (5-6 keV rms) at the injector, using a laser heater (LH) system [3] at 100 MeV.

The linac is segmented into several sections in order to include two magnetic chicanes to compress the bunch to a 1-kA peak current (8.6 micron rms bunch length at 100 pC). The linac segments and their various parameters are summarized in Figure 2, including the beam energy, rms bunch length, rms relative energy spread, chicane strength (R_{56}), RF phases, crest voltage, and cryomodule number. The RF parameters are in Table 1.

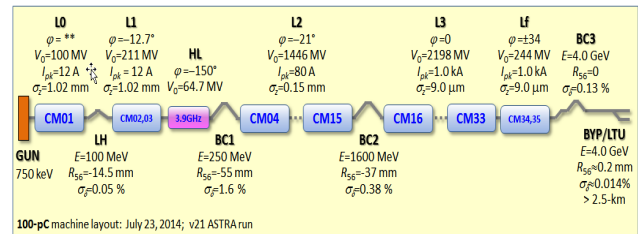


Figure 2: Linac layout with RF and compression parameters.

Table 1: SC-linac RF Parameters at 100 pC/bunch

Linac section	Phase (deg)	Gradient (MV/m)	No. of CM's	Avail. cavities	Powered cavities
L0	~0	16.3	1	8	7
L1	-12.7	13.6	2	16	15
HL	-150	12.5	2	16	15
L2	-21	15.5	12	96	90
L3	0	15.7	18	144	135
Lf	±34	15.7	2	16	15

The average accelerating gradient (for most 1.3-GHz cavities) has been chosen at ~ 16 MV/m with an unloaded Q value of $\geq 2.7 \times 10^{10}$ at a temperature of 2.0 K. The RF parameters in Table 1 assume 6% of all cavities nominally unpowered as spares (or in maintenance), and the mean accelerating gradient is defined over the powered cavities only, and at crest phase. The “Lf” section is just the last two cryomodules arranged with a nominal $+34^\circ$ and -34° phasing, as opposed to L3 with 18 CM’s at crest phase. The Lf section provides an electron energy adjustment range of $\pm 1\%$, which will be controlled by an energy feedback loop. Keeping the two phases equal but opposite in sign (symmetric around crest phase) eliminates the induced energy chirp along the bunch, and provides energy control with these two phase settings.

ELECTRON BEAM PARAMETERS

A list of electron beam parameters is given in Table 2, including the *nominal* parameters and their ranges (range values are not simultaneous here).

Table 2: Electron Beam Parameters (Nominal and Range)

Parameter	sym.	nom.	range	unit
Final energy	E_f	4.0	2.0-4.1	GeV
Bunch charge	Q_b	100	10-300	pC
CW linac bunch rate	f_b	0.62	0-0.93	MHz
Avg. linac current	I_{av}	62	1-300	μ A
Avg. linac e^- power	P_{av}	0.25	0-1.2	MW
Emittance (norm., x & y)	$\gamma\epsilon_{1-2}$	0.45	0.2-0.7	μ m
Final peak current	I_{pk}	1.0	0.5-1.5	kA
Final rms bunch length	σ_{zf}	8.6	0.6-52	μ m
Compression factor*	C_T	85	25-150	-
Final slice E -spread, rms	σ_{Es}	500	125-1500	keV

* Total magnetic, from injector-end (100 MeV) to undulator.

FOCUSING LATTICE

The linac focusing lattice (L1, L2, and L3) is set using cold quadrupole magnets at the end of each 13-m CM, with some warm quadrupole magnets included around the bunch compressors to match the Twiss functions. The linac focusing lattice ($30^\circ/\text{cell}$, L2 & L3), from cathode to HXR dump, is shown in Figure 3. The lines split in two (to HXR or SXR lines) at $s \approx 2776$ m (kicker).

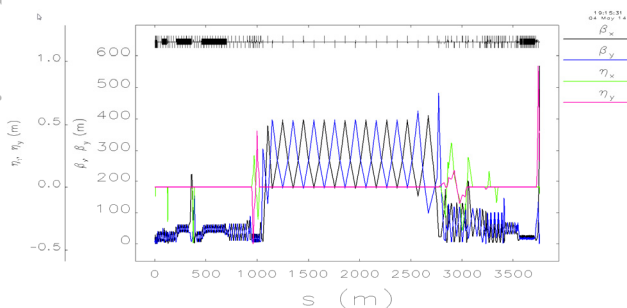


Figure 3: Focusing lattice from cathode to HXR dump. Large beta functions are in the existing, long bypass line,

while the HXR undulator is near the end of the line at $s \approx 3550$ -3700 m.

Similarly, the focusing over the full SXR-machine, from cathode to SXR dump, is shown in Figure 4. This plot is different from the previous plot only at $s > 2776$ m.

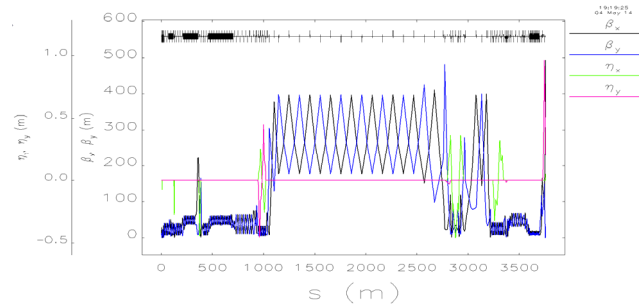


Figure 4: Focusing lattice from cathode to SXR dump at 4 GeV. The SXR undulator is near the end of the line at $s \approx 3600$ -3700 m. The two lines split (to HXR or SXR) at $s \approx 2776$ m.

ELECTRON DIAGNOSTICS

The high-rate and high-power electron beam in the SC-linac makes intercepting diagnostics (*e.g.*, beam screens) difficult to use without damage. For this reason an off-axis (parallel) diagnostic section is tapped off the main linac just after the laser heater at 100 MeV using a fast kicker to steal pulses at up to 100 Hz (< 15 W). This post-LH diagnostic section includes a transverse RF deflector allowing both projected and slice measurements for emittance and energy spread continuously.

Existing strip-line BPMs are used in most locations with cold button-BPMs used at the end of each CM. Cavity BPMs are used in several key locations for feedback control and in the undulators where a 1-2 μ m rms position resolution is required. Relative bunch length monitors (coherent edge radiation) are included after each bunch compressor, similar to that used in LCLS-I [4]. Fast wire-scanners (~ 1 m/s) are envisioned for transverse beam profiles and emittance measurements at several in-line locations along the machine. YAG and OTR screens may be included, but are presently compromised in performance by coherent transition radiation. Finally, RF deflectors will be used to time-resolve key emittance and energy spread measurements, as allowed by budget.

LONGITUDINAL STABILITY

The jitter of the linac RF systems will cause the final bunch characteristics to vary, affecting the FEL performance. The variable bunch characteristics are primarily: 1) the final electron energy, 2) the final peak current, and 3) the arrival time of the bunch in the undulator. We therefore require specific stability tolerances for each RF system (phase and amplitude), bunch charge, drive-laser timing, and bunch compressor chicane power supplies, such that the final machine stability is within our chosen limits. These limits are as

follows: *a*) a final relative electron energy stability of $< 0.01\%$ rms, *b*) a final relative peak current stability of $< 4\%$ rms, and *c*) an arrival time of the electron bunch (assumed same as x-ray pulse timing) of < 20 fs rms.

To prescribe the necessary RF tolerances we first need to calculate the individual error sensitivities, defined as the level of error required to change each of the bunch characteristics by exactly the chosen limits. For example, we calculate the L2-linac RF phase error ($\Delta\phi_2$), assuming all 90 powered RF cavities in L2 vary in an uncorrelated and random way, which causes: 1) an energy change of 0.01%, 2) a peak current change of 4%, and 3) a timing change of 20 fs (each individually, not simultaneously).

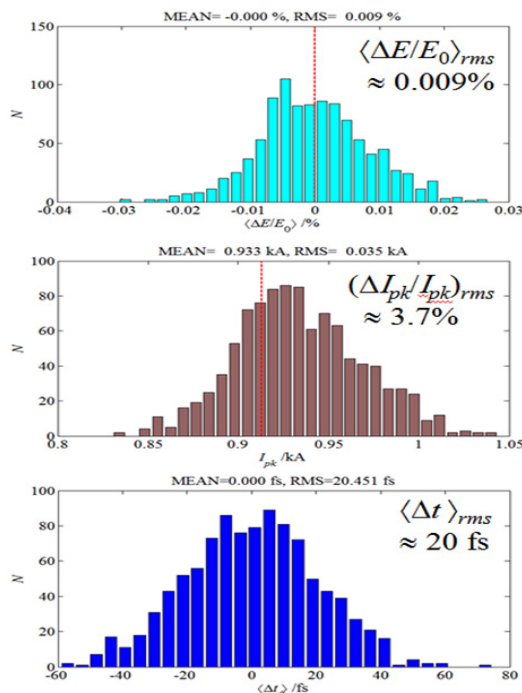


Figure 5: Jitter/tracking simulation using *LiTrack* [5] and rms (Gaussian) stability tolerances of Table 3, confirming the final expected stability of $(\Delta E/E)_{rms} \approx 0.009\%$, $(\Delta I_{pk}/I_{pk})_{rms} \approx 3.7\%$, and $\Delta t_{rms} \approx 20$ fs rms. It may be possible to improve this.

Of course the sensitivities are not applicable as system tolerances, since each one (by itself) consumes the entire stability budget. For this reason, we scale down each sensitivity such that the quadrature sum of all errors, assuming uncorrelated jitter from system to system, just reaches the beam stability limit for each item. The list of final rms tolerances as a full stability budget is given in Table 3, where we assume uncorrelated errors over the “ N cavities” in each linac section, assuming each cavity is powered by its own RF power amplifier. Note also that beam-based feedback systems will stabilize these errors at frequencies below ~ 1 Hz, so these tolerances represent the fast jitter levels that must not be exceeded by design. Final tracking simulations, with rms jitter on each item as listed in Table 3, are shown in Figure 5 as verification.

Table 3: Longitudinal Stability Tolerances at 100 pC/bunch

Parameter (rms)	symbol	Tol.	N cav's	unit
Phase error in L0	$\Delta\phi_0$	0.040	7	degL
Phase error in L1	$\Delta\phi_1$	0.039	15	degL
Phase error in HL	$\Delta\phi_H$	0.039	15	degH
Phase error in L2	$\Delta\phi_2$	0.095	90	degL
Phase error in L3-linac	$\Delta\phi_3$	1.8	150	degL
Amplitude error in L0	$\Delta V_0/V_0$	0.026	7	%
Amplitude error in L1	$\Delta V_1/V_1$	0.039	15	%
Amplitude error in HL	$\Delta V_H/V_H$	0.039	15	%
Amplitude error in L2	$\Delta V_2/V_2$	0.095	90	%
Amplitude error in L3	$\Delta V_3/V_3$	0.12	150	%
Laser timing error*	Δt_c	0.31	-	ps
Bunch charge error	$\Delta Q/Q_0$	1.5	-	%
Current reg. in LH	$\Delta I_H/I_H$	0.005	-	%
Current reg. in BC1	$\Delta I_1/I_1$	0.005	-	%
Current reg. in BC2	$\Delta I_2/I_2$	0.003	-	%

* The gun timing error is compressed by 3.85, from gun to 100 MeV, due to velocity compression.

WAKEFIELDS OF LONG TRANSPORT

The long transport lines following the LCLS-II linac also generate longitudinal wakefields which need to be included in the bunch compression system design, especially for cancellation of the energy chirp before entering the FEL. The wakefields are due to the resistive-wall effect and have contributions from each transport line section according to pipe radius, material, and length. The various wakefield section parameters are listed in Table 4, including pipe length, internal radius, internal plating material, and the material’s conductivity. The DC wakefield is accurate here, ignoring AC conductivity [6]. Beamline sections of Table 4 are labeled in Figure 1.

Table 4: Resistive-Wall Wakefields of Long Transport Lines

Beamline Section	Pipe Length (m)	Pipe Radius (mm)	Pipe Material	Cond. / 10^6 (Ohm-m) $^{-1}$
Linac Exten.	250	24.5	stainless	1.37
Dog-Leg #1	78	19	stainless	1.37
Bypass Line	1734	24.5	stainless	1.37
LTU-SXR	827	24.5	Alum.	36.0
LTU-HXR*	778	20.6	Copper	58.0

* Much of this pipe exists and is copper plated to reduce wakes.

BEAM SPREADER AND BEAM DUMPS

To rapidly switch beam into one of two FEL undulators, a fast, bipolar, vertical magnetic kicker (0.75 mrad) is used at the end of the bypass line at up to a 1-MHz switching rate. The kicker requires 50 ppm rms field stability and < 40 nrad rms kick variation at baseline (no kick). Two 2-hole horizontal Lambertson magnets

(septa) then spread the beam to the HXR or SXR undulators as shown in Figure 6 and Figure 7.

Electron beam dumps at the end of each FEL line are limited to 120 kW of beam power. Therefore, at a 100-pC bunch charge and 4 GeV, the maximum repetition rate in each FEL line is 312 kHz. With a lower bunch charge (e.g., 30 pC) the rate can be increased to 1 MHz, but always power-limited to 120 kW in each FEL line.

The linac beam power can be twice this level (250 kW at 625 kHz for 100 pC/bunch) and a straight-ahead beam dump, “D10” in Figure 6, is included after the spreader (kicker off). This dump is rated for 250 kW and will reuse the existing MW-class dump presently in the linac.

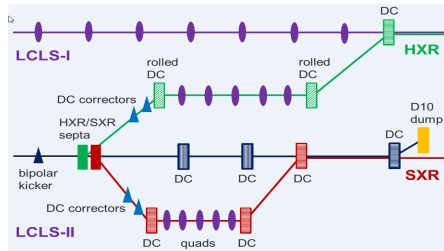


Figure 6: Fast beam spreader system (plan view) with vertical “kicker” and two “2-hole septa” magnets which bend horizontally. This schematic shows the geometry rather than the complete optics (e.g., not all quads are shown).

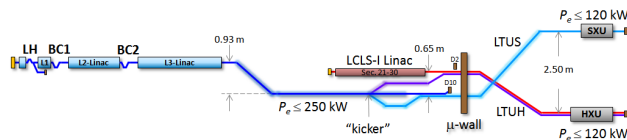


Figure 7: Full LCLS-II layout (plan view) with switching into the SXR undulator (top-right) and HXR undulator (lower-right) at up to a 1-MHz rate using a fast “kicker” and two septa.

BEAM COLLIMATION

Included in the linac layout is a system of adjustable-gap collimators designed to block undesirable beam halo which might otherwise be lost in radiation sensitive areas. It is designed to greatly reduce the rate of undulator demagnetization caused by beam-loss induced radiation, and to limit beam loss to below 1 W/m in areas with limited radiation shielding. The system employs multiple stages of collimation in x , x' , y , y' , and δ , phase space coordinates. Simulations show the gun-generated halo can be reduced by a more than factor of 10^7 . Touschek and beam-gas-generated halo, which are expected to be significant but at a much lower level than gun-generated halo, are also seen to be well collimated before reaching the undulator.

MICROBUNCHING INSTABILITY

The microbunching instability can have a significant impact on beam quality causing, in particular, an undesired growth in the sliced beam energy spread. The primary means to control the instability is the laser heater

(LH). The current LH design uses the same undulator as in LCLS-I ($\lambda_u = 5.4$ cm), but with longer laser wavelength ($\lambda_L = 1$ μm) to exploit the availability of high rep-rate, high-power systems. For the 100-pC baseline beam, an estimate based on linear theory for the microbunching instability indicates an optimum LH setting corresponding to 5-6 keV rms energy spread at 100 MeV, consistent with a 500-600 keV rms sliced energy spread at the FELs ($C_T \approx 100$). Preliminary results (to be reported elsewhere) from high-resolution macro-particle simulations with *IMPACT* [7], fully accounting for CSR and space charge fields, show a somewhat larger effect of the instability, which appears to be noticeably aggravated by the presence of the long transport sections between the SC-linac and the FELs. The *IMPACT* simulations also allow for an accurate characterization of the so-called “trickle-heating” effect [3], due to space charge and the micro-correlations induced by the electron/laser interaction in the LH. The effect (see Figure 8) may not necessarily be harmful but it interferes with the ability to control the induced energy spread by appropriate tuning of the laser power, especially at low settings. Possible remedies include a modification of the LH chicane, machine lattice, or less desirably, choice of the LH laser wavelength (shorter).

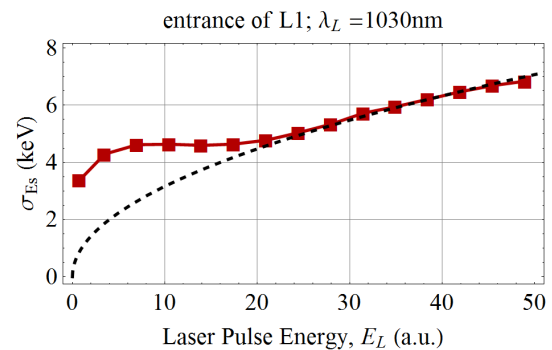


Figure 8: The beam slice energy spread ($Q = 100$ pC) as observed at the entrance of L1 (*IMPACT* simulations) deviates from $\sim\sqrt{E_L}$ (dashed line) because of the “trickle heating” effect. (Here, the beam time-slice is defined to be a few μm 's long.)

START-TO-END TRACKING RESULTS

Start-to-end particle tracking simulations have been done using *Elegant* [8] and *ASTRA* [9], where *ASTRA* tracks from cathode through first CM at 100 MeV, including space-charge forces. *Elegant* takes this beam and continues tracking through the full linac, the long transport lines, and to the start of the undulators, including bunch compression, 2nd-order optics, longitudinal wakefields of the linac and long transport-lines, plus coherent radiation (CSR) in the bends using a transient 1D line-charge model. The final longitudinal phase space at 4 GeV is shown in Figure 9. The slice emittance (0.35 μm at 100 pC here) is not increased while the flat energy profile (middle) is the result of the resistive-wall wakefields in the long transport lines described above.

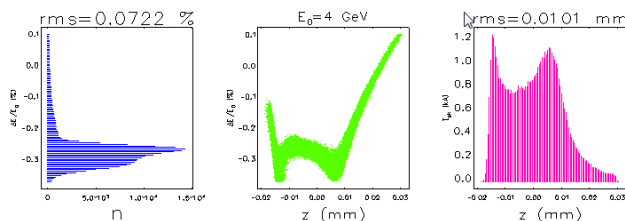


Figure 9: *Elegant* tracking results of longitudinal phase space (100 pC/bunch) including resistive-wall wakes and CSR in the bends. Space charge is only included in the *ASTRA* tracking.

SUMMARY

The baseline design of the LCLS-II CW, SC linear accelerator generates the appropriate beam power, rate, and quality for the two new FELs to be built at SLAC. The detailed particle tracking up to high energy has not yet included space-charge forces, which may be a beam quality limitation with regard to the micro-bunching instability. The design study continues.

REFERENCES

- [1] T. Raubenheimer, “The LCLS-II, a New FEL Facility at SLAC”, in *Proc. of 36th Int. Free-Electron Laser Conf.*, Basel, Switzerland, 2014, WEB001.
- [2] J. Schmerge *et al.*, “The LCLS-II Injector Design”, in *Proc. of 36th Int. Free-Electron Laser Conf.*, Basel, Switzerland, 2014, THP042.
- [3] Z. Huang *et al.*, “Measurements of the Linac Coherent Light Source Laser Heater and its Impact on the X-ray Free-Electron Laser Performance”, *Phys. Rev. ST - AB*, **13**, 020703 (2010).
- [4] H. Loos, “LCLS Accelerator Operation and Measurement of Electron Beam Parameters Relevant for the X-ray Beam”, *Proc. SPIE 8778, Advances in X-ray Free-Electron Lasers II: Instrumentation*, 87780J (May 3, 2013), doi:10.1117/12.2021569.
- [5] K. Bane, P. Emma, “*LiTrack*: A Fast Longitudinal Phase Space Tracking Code with Graphical User Interface”, in *Proc. of 2005 Part. Acc. Conf.*, Knoxville, TN, USA, pp. 4266-4268, 2005.
- [6] K.L.F. Bane, G. Stupakov, “Resistive Wall Wakefield in the LCLS Undulator Beam Pipe”, SLAC-PUB-10707, October 2004.
- [7] J. Qiang, *et al.*, “High Resolution Simulations of Beam Dynamics in Electron Linacs for X-ray Free-Electron Lasers”, *Phys. Rev. ST-AB*, **12**, 100792, (2009).
- [8] M. Borland, *Elegant*, APS LS-287, presented at ICAP 2000, Darmstadt, Germany.
- [9] K. Floettmann, “Astra”, DESY, Hamburg, <http://www.desy.de/~mpyflo>, 2000.